ACS Catalysis

Research Article

pubs.acs.org/acscatalysis

Ternary VZrAlON Oxynitrides - Efficient Catalysts for the Ammoxidation of 3-Picoline

Christiane Janke,[†] Jörg Radnik,[‡] Ursula Bentrup,[‡] Andreas Martin,[‡] and Angelika Brückner*[,‡]

[†]BASF SE, GCC/PG-M301, 67056 Ludwigshafen, Germany

[‡]Leibniz Institut für Katalyse e.V. an der Universität Rostock, Albert-Einstein-Straße 29a, Rostock, 18059 Germany

Supporting Information

ABSTRACT: Starting from previous binary VZrON (VAlON) oxynitrides with high (low) activity and low (high) selectivity, a new class of ternary VZrAlON catalysts has been developed for the ammoxidation of 3-picoline to 3-cyanopyridine (3-CP), which combine the beneficial properties of the binary oxynitrides, leading to improved selectivity at retained high activity and to the highest space-time yield of 3-CP ever measured (488 g L^{-1} h^{-1}). This is attributed to the formation of a special $-\square-V^{5+}(O)-N-Al(Zr)-$ surface moiety consisting of a $V^{5+}{=}O$ species in the vicinity of a surface nitrogen and an anion vacancy occupied by an electron, which is supposed to provide optimum conditions for a double Mars–van Krevelen mechanism comprising activation of gas-phase oxygen and ammonia via reversible incorporation into the catalyst surface as well as an efficient electron transport.

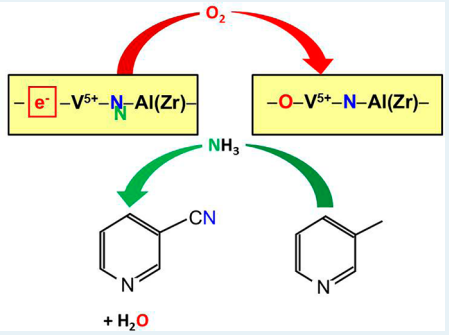

KEYWORDS: *ammoxidation, 3-picoline, vanadium zirconium aluminum oxynitrides, in situ EPR spectroscopy, XPS, UV–vis spectroscopy, structure–reactivity relationships*

INTRODUCTION

The gas-phase ammoxidation of methylaromatics and heteroaromatics is an ecologically and economically efficient route to synthesize a variety of different nitriles (eq 1), as long as high nitrile selectivities and space-time yields (STY) are reached.[1,2] Thus, 3-cyanopyridine (3-CP, also known as nicotinonitrile), being the source for the production of vitamin B3, is obtained by ammoxidation of 3-picoline over a variety of vanadium-containing oxide catalysts such as VPO,[3−5] VTiO,[6] VSnO[7] or VSbTiO.[8]

$$R - CH_3 + NH_3 + 3/2O_2 \rightarrow R - CN + 3H_2O \quad (1)$$

With binary VAlON and VZrON oxynitrides[9] we could achieve almost 3 times higher STY of 3-CP as obtained with an industrial SbVTiSiKO benchmark catalysts.[10] A maximum STY of 399 g/L h was reached with VZrON catalysts, yet the 3-CP selectivity did not exceed 63% at a conversion of 91%. On the other hand, VAlON catalysts were found to be more selective but less active than VZrON materials ($X_{3\text{-PIC}}$ = 80%, $S_{3\text{-CP}}$ = 79%).[9] Structural differences have been identified as major reasons for this. Thus, it was found that VZrON catalysts contain mainly polymerized VO_x species with a high mean valence state (close to +5) and almost no nitrogen on the surface under working conditions. In contrast, for VAlON catalysts not only a lower V site agglomeration and a lower mean surface V oxidation state but also its ability to incorporate nitrogen species in the surface has been evidenced. These properties were regarded as crucial for high 3-CP selectivity, since it had been shown previously that single VO^{2+} sites suppress total oxidation of hydrocarbons to CO_x and incorporation of N into the catalyst lattice enables a so-called double Mars–van-Krevelen mechanism for the activation of both oxygen and ammonia.[11] On the basis of a comprehensive analysis of structure–reactivity relationships, it has been concluded that highly selective and active ammoxidation catalysts must be able to reversibly incorporate N into their surface and must expose highly dispersed V species with a mean surface valence state close to +4 as well as V and N surface sites in close vicinity (preferentially as V–N–M moieties).[9] Moreover, they should be free of pronounced surface acidity.[9] Attempts to adjust such properties in VZrPON catalysts were not successful since the incorporation of P, though enhancing the V site dispersion, led to a detrimentally high surface acidity.[12]

In this work, we follow a new approach aimed at combining the beneficial properties of both binary catalysts systems. The objective was to develop a novel class of ternary VZrAlON catalysts which maintain the high activity of VZrON and the high selectivity of VAlON. Here we show that this approach was indeed successful, leading to ammoxidation catalysts with significantly improved catalytic properties. Besides, relations between structural peculiarities and catalytic performance have been established using a variety of analytical techniques (XRD, XPS, ATR, UV–vis–DRS) as well as by monitoring the nitridation and ammoxidation process with in situ EPR spectroscopy.

Received: April 7, 2014
Revised: June 13, 2014
Published: July 5, 2014

   dx.doi.org/10.1021/cs500458w | ACS Catal. 2014, 4, 2687−2695

EXPERIMENTAL SECTION

Catalyst Preparation. The VZrAlO-*x* oxide precursors, in which *x* denotes the theoretical V/(Al+Zr) ratio established during synthesis from 0.1 to 0.6 at a constant Al/Zr ratio of 1.5, were synthesized by coprecipitation. The desired amount of NH_4VO_3 (Aldrich, 99%) was suspended in distilled water (0.1 M) at 70 °C and subsequently acidified with 65% HNO_3 (Roth, pure) at 70 °C under stirring to reach a final pH of 3. In a second solution, $Al(NO_3)_3 \cdot 9\ H_2O$ (Sigma-Aldrich, 98%) and $ZrO(NO_3)_3$ (Aldrich, tech.) were dissolved in distilled water at 70 °C under stirring, adjusting a concentration of 0.15 M for each component. The hot NH_4VO_3 solution was slowly added to the hot Al−Zr solution. Subsequently, the pH of the final solution was raised to 7 at 70 °C by slowly adding NH_4OH (Merck, 25%). This led to the formation of a yellow precipitate, which was filtered, washed twice with distilled water, dried at 120 °C for 16 h and finally ball-milled to obtain a fine yellow powder of the VZrAlO-*x* oxide precursor. About 6 g of each VZrAlO precursor was heated with 5 K/min in NH_3 flow (3.8, Air Liquide, 30 L/h) to 600 °C and nitrided for 6 h, resulting in black VZrAlON-*x* oxynitride powders.

Catalytic Tests. Catalytic tests were performed in a fixed bed glass reactor with an inner diameter of 1.5 cm. Oxynitride powders were pressed to pellets, crushed, and sieved. Catalyst particles of 1.0−1.25 mm size were diluted with glass beads (1.25−1.55 mm) in a volumetric ratio of 1:1.7 for each test. The reaction temperature T_B was measured inside the catalyst bed by a thermocouple. Air (5.0, Air Liquide) and ammonia (3.8, Air Liquide) were dosed by mass flow controllers (Bronkhorst). Water and 3-picoline (Aldrich, 99%) were premixed and fed continuously into the gas stream by a syringe pump. The molar ratio of the feed components was set to 3-PIC/air/NH_3/H_2O = 1/28/5/8. Prior to each catalytic test, the catalyst inside the reactor was heated with 10 K/min in air/NH_3 flow to 190 °C, and subsequently the 3-PIC and H_2O were added. The gas stream leaving the reactor outlet was trapped in ethanol. Concentrations of 3-PIC and 3-CP were analyzed off-line using a GC-17A (Shimadzu) equipped with an autosampler, a WCOT fused silica CP-SIL 8 CB column (Varian), and an FID. Concentrations of the byproducts CO_2 and CO were analyzed online using a nondispersive infrared analyzer (BINOS 100 2M, Rosemount). Catalytic tests of VZrAlON-*x* were performed at two different gas hourly space velocities (GHSV), either at 2713 h^{-1} or at 5728 h^{-1}. The reaction temperature T_B was varied between 320 and 390 °C. Carbon balances were calculated for each test to judge the quality of the catalytic test results.

Catalyst Characterization. Elemental compositions were determined by ICP-OES and CHN analysis. ICP-OES measurements were performed with a Varian 715-ES spectrometer. Ten mg of the catalyst was dissolved in 4 mL HF and 4 mL aqua regia. These solutions were treated in a microwave (Anton Paar/PerkinElmer) at ca. 60 bar and 120 °C, diluted to 100 mL, and measured. CHN analyses of 10−30 mg powder samples were performed with an EA 1110 CHN analyzer (CE Instrumenta) using a tin crucible. All values were verified by double determination. BET surface areas (S_{BET}) were measured by krypton adsorption at 77 K using an ASAP2010 setup.

Powder XRD patterns were recorded with Cu Kα1 radiation on a Stoe STADI P diffractometer. Processing and assignment of the powder patterns was done using the software Win X Pow (Stoe) and the powder diffraction file (PDF) database of the International Center of Diffraction Data (ICDD).

X-ray photoelectron spectra (XPS) were recorded on a VG ESCALAB 220iXL instrument with Mg Kα radiation. The peaks were fitted by Gaussian−Lorentzian curves after a Shirley background subtraction. The electron binding energies E_B were referenced to the carbon 1s peak at 284.8 eV. For quantitative analysis, the peak areas were determined and divided by the element-specific Scofield factors and the analysator-depending transmission function.

FTIR spectra at ambient conditions were recorded in the attenuated total reflection (ATR) mode using an Alpha-P FTIR spectrometer (Bruker).

EPR spectra in X-band ($\nu \approx 9.5$ GHz) were recorded on an ELEXSYS 500-10/12 cw spectrometer (Bruker) using a microwave power of 6.3 mW, a modulation frequency of 100 kHz, and a modulation amplitude of 0.5 mT. The magnetic field was measured with respect to the standard, 2,2-diphenyl-1-picrylhydrazyl. For in situ experiments, a homemade quartz plug-flow reactor connected to a gas/liquid-dosing system (equipped with mass flow controllers for gases and saturators for liquids) was implemented in the rectangular cavity of the spectrometer.[13] The reactor was loaded with 100 mg of catalyst particles (315−710 μm). After heating in air/NH_3 (4.5/1) to 350 °C, H_2O was introduced at the same temperature. Subsequently, 3-PIC was added (3-PIC/air/NH_3/H_2O = 1/30/6/8) and switched off again after a certain time. At the end of the experiments, the gas feed was changed to pure N_2, and the reactor was cooled to room temperature (RT). EPR spectra at 350 °C were recorded until reaching a steady state. Besides interaction of the oxynitrides with feed components, also the reaction of the VZrAlO-0.5 oxide precursor with NH_3 was monitored by EPR. In this case, 112 mg particles were first heated from RT to 120 °C in N_2 (10 mL/min) and cooled again to RT. Then, the gas flow was switched to 20% NH_3/N_2 (38 mL/min) at RT, and the reactor was heated stepwisely to a final temperature of 410 °C. Spectra at elevated temperatures were recorded as a function of time for at least 30 min. Computer simulation of EPR spectra was performed with the program SIM14S of Lozos et al.[14] using the spin Hamiltonian (eq 2)

$$H = \mu_B S\mathbf{g}B_o + S\mathbf{A}I \tag{2}$$

in which the symbols have the following meaning: μ_B - Bohr magneton, **g** - **g** tensor, **A** - hyperfine tensor, *S* - electron spin operator, *I* - nuclear spin operator and B_o - magnetic field vector. The parameter $\Delta g_\parallel/\Delta g_\perp$, being a measure of the axial distortion of the VO^{2+} site was derived by eq 3

$$\Delta g_\parallel/\Delta g_\perp = (g_\parallel - g_e)/(g_\perp - g_e) \tag{3}$$

in which $g_\parallel$ and $g_\perp$ are the parallel and perpendicular components of the axial **g** tensor and g_e is the *g* value of the free electron (g_e = 2.0023). The in-plane delocalization coefficient $\beta_2{}^{*2}$ was calculated according to eq 4,[15] in which $A_\parallel$ and $A_\perp$ are the principal components of the hyperfine structure (hfs) tensor and P = 184.5 G is the term for the dipole−dipole interaction of the magnetic moment of the electron and the nucleus for the free V(IV) ion.[16]

$$\beta_2{}^{*2} = 7/6\Delta g_\parallel - 5/12\Delta g_\perp - 7/6[(A_\parallel - A_\perp)/P] \tag{4}$$

RESULTS AND DISCUSSION

Catalytic Performance. Conversion of 3-PIC ($X_{3\text{-PIC}}$) and selectivity of 3-CP ($S_{3\text{-CP}}$) have been measured at two different space velocities (GHSV = 2713 h^{-1} and 5728 h^{-1}) as a function of the experimental bulk V/(Al+Zr) ratio determined by ICP (Figure 1 A and B). In general, catalysts have been tested on stream for about 6 h. No deactivation was observed during this time. The experimental error was ±2% for selectivity and even lower for conversion values. The carbon balance was always in the range of 96−101%. The bed temperature T_B was adjusted to 360 °C for both space velocities. As expected, the higher the space velocity the lower $X_{3\text{-PIC}}$ and the higher $S_{3\text{-CP}}$. In general, almost equal trends are observed. The $X_{3\text{-PIC}}$ values pass a maximum at a $V/(Al+Zr)_{ICP}$ ratio of around 0.5, while the $S_{3\text{-CP}}$ increases almost linearly with rising $V/(Al+Zr)_{ICP}$ ratio for both high and low GHSV. The best catalytic performance, judged by the yield $Y_{3\text{-CP}}$, was obtained with catalyst VZrAlON-0.5 while sample VZrAlON-0.1 showed the lowest performance. The marked drop of conversion for the catalyst with V/(Al+Zr) = 0.6 is most probably due to its much lower surface area (S_{BET} = 55.4 $m^2\ g^{-1}$) in comparison to that of the other catalysts (Table 1). Therefore, detailed characterization studies described below have been focused on these two catalysts.

dx.doi.org/10.1021/cs500458w | ACS Catal. 2014, 4, 2687−2695

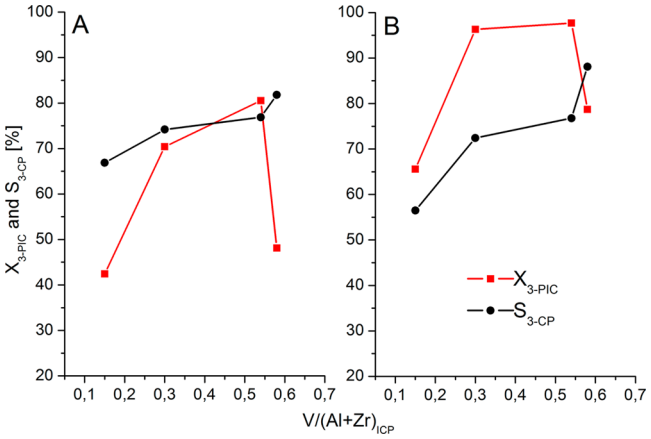

Figure 1. Catalytic performance of VZrAlON catalysts measured at a bed temperature of T_B = 360 °C and space velocities of GHSV = 5728 h^{-1} (A) and 2713 h^{-1} (B) as a function of the V/(Al+Zr)$_{ICP}$ ratio.

Table 1. Bulk and Surface V/(Al+Zr), Al/Zr, and N/V Elemental Ratios, N Contents and Specific Surface Areas (S_{BET}) of the Fresh and Used Catalysts[a]

sample	V/(Al+Zr)	Al/Zr	N/V	N [wt %]	S_{BET} [m^2/g]
VZrAlON-0.1 fresh	0.15 (0.10)	1.55 (1.99)	0.68 (0.00)	1.51	199
VZrAlON-0.1 used	0.16 (0.09)	1.54 (1.85)	0.44 (0.70)	0.84	167
VZrAlON-0.5 fresh	0.54 (0.20)	1.51 (1.96)	0.54 (0.35)	3.07	153
VZrAlON-0.5 used	0.52 (0.28)	1.52 (2.17)	0.34 (0.32)	1.84	110

[a]Surface ratios derived by XPS are given in brackets. Bulk ratios and N contents were obtained from ICP-OES and CHN analysis, respectively.

In Figure 2, conversion and selectivity for the best catalysts from the binary VAlON and VZrON series (values for VZrON-0.25 and VAlON-0.5 taken from ref 9) are compared with the values measured for the best catalyst of the ternary VZrAlON series studied in this work. As already described in ref 9, the VZrON-0.25 catalyst shows a much higher 3-PIC conversion but lower 3-CP selectivity than catalyst VAlON-0.5. For this reason the space velocity had to be raised to 5728 h^{-1} for VZrON catalysts, to control the exothermicity of the reaction and to minimize undesired total oxidation to CO_x.

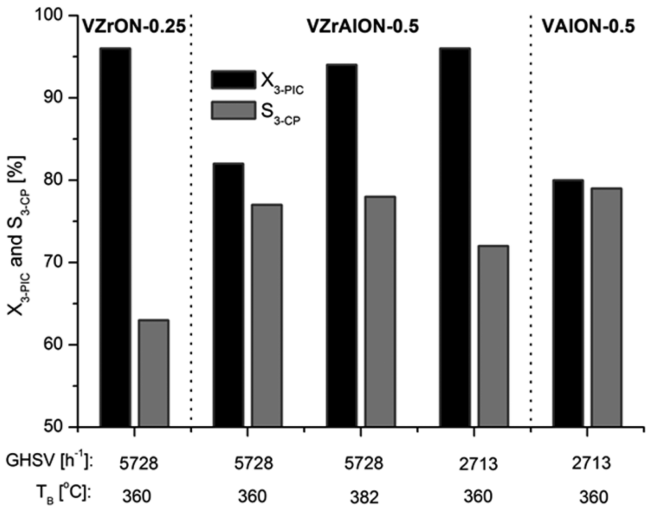

Figure 2. Conversion ($X_{3\text{-PIC}}$) and selectivity ($S_{3\text{-CP}}$) at different bed temperatures (T_B) and space velocities (GHSV) for the VZrON-0.25, VZrAlON-0.5, and VAlON-0.5 catalysts. Values of VZrON-0.25 and VAlON-0.5 are taken from ref 9.

Interestingly, addition of Zr to VAlON-0.5 improves the activity but lowers also the selectivity, as can be seen from a comparison of VAlON-0.5 and VZrAlON-0.5 under the same reaction conditions at T_B = 360 °C and GHSV = 2713 h^{-1} (Figure 2). However, at almost equal conversion (82% for VZrAlON-0.5 and 80% VAlON-0.5) which was reached at the same bed temperature of 360 °C but with different space velocities, VZrAlON-0.5 is only marginally less selective than VAlON-0.5. Interestingly, for VZrAlON-0.5 a 2-fold higher GHSV could be applied, which enabled a markedly higher STY without significant loss of selectivity compared to that with VAlON-0.5. Catalysts VZrAlON-0.5 and VZrON-0.25 reach almost the same conversion (96 vs 94%) at a GHSV of 5728 h^{-1}. However, a higher bed temperature of 382 °C was needed for sample VZrAlON-0.5 compared to that for catalyst VZrON-0.25 (360 °C), since the former catalyst is less active (but more selective).

Nevertheless, a remarkable improvement of the space-time yield (STY) was achieved with the ternary VZrAlON-0.5 catalyst. Its maximum value of 488 g L^{-1} h^{-1} is now the highest STY ever measured in gas-phase ammoxidation of 3-PIC to 3-CP and markedly exceeds our previous result of STY = 399 g L^{-1} h^{-1} obtained for the binary VZrON-0.25 catalysts[9]. To elucidate possible structural reasons for these differences, the best and the worst ternary VZrAlON catalysts have been comprehensively characterized ex situ before and after use in the catalytic reaction as well as by in situ EPR during ammoxidation. Additionally, the latter technique was also applied to follow nitridation of the respective oxide precursors in NH_3 flow. The obtained results are discussed in comparison to those of the binary VZrON and VAlON materials already published in ref 9.

Bulk and Surface Composition and Structure of VZrAlON-0.1 and VZrAlON-0.5 Catalysts. Both catalysts do not show any reflections in the XRD powder patterns neither before nor after use in the ammoxidation reaction. This indicates that they are X-ray-amorphous and the incorporation of Zr does not lead to crystallization of ZrO_2 as observed previously in binary VZrON samples,[9] but rather to a well intermixed Zr−O−Al network. The bulk properties and surface elemental ratios for fresh and used VZrAlON samples are listed in Table 1.

It is obvious that the V/(Al+Zr) ratios on the surface are lower than those in the bulk, indicating that vanadium is partially enriched in the volume of the catalysts. The opposite trend is observed for the Al/Zr ratios, suggesting that Al sites are more abundant on the surface. However, both the V/(Al+Zr) as well as the Al/Zr ratios do not change much for both catalysts after use in the catalytic reaction, neither in the bulk nor on the surface. More significant are differences related to the nitrogen content. It can be seen that the amount of incorporated nitrogen increases with the total V content suggesting that V and N sites might be related to each other, yet about 40% of the nitrogen incorporated during the nitridation process is lost after ammoxidation catalysis for both fresh catalysts. Interestingly, the surface N/V ratio stays

dx.doi.org/10.1021/cs500458w | ACS Catal. 2014, 4, 2687−2695

Table 2. Binding energies E_B [eV] and surface percentages (given in brackets) for fresh and used VZrAlON catalysts derived from XPS

sample	Al 2p	Zr $3d_{3/2}$	N 1s[a]	V $2p_{3/2}$[a]	ΔE_B[b]	mean V valence[c]
VZrAlON-0.1 fresh	72.8 (19.5)	181.1 (12.3)	–	517.1 (3.6)	13.6	4.3
VZrAlON-0.1 used	73.8 (15.5)	181.8 (10.8)	399.5 (2.0)	516.6 (2.8)	13.3	4.5
VZrAlON-0.5 fresh	73.8 (12.7)	182.0 (10.9)	397.6 (1.2)	516.8 (3.8)	14.3	3.8
			401.0 (0.6)	518.2 (2.7)	12.9	4.8
			403.4 (0.6)			
VZrAlON-0.5 used	74.7 (8.0)	182.5 (7.5)	399.2 (1.2)	514.8 (2.6)	14.8	3.4
			400.8 (1.0)	517.4 (4.1)	12.2	5.2

[a]Values in brackets denote the ratio between different species of the same element. [b]$\Delta E_B = E_B(O\ 1s) - E_B(V\ 2p_{3/2})$. [c]Derived from ΔE_B (see ref 31).

almost the same before and after use for VZrAlON-0.5. In contrast, no surface N sites are detected in fresh VZrAlON-0.1. This may be due to the fact that the surface V content of sample VZrAlON-0.1 is much smaller than that of VZrAlON-0.5. Thus, the number of V sites on the surface of VZrAlON-0.1 might be too small for stabilizing sufficient N surface sites that exceed the detection limit of XPS. Interestingly, surface N sites in sample VZrAlON-0.1 become abundant after use—in contrast to the binary VZrON catalysts, in which no surface N species could be detected neither before nor after their use in the catalytic reaction.[9] This suggests that the incorporation of Al in the surface of VZrAlON catalysts favors the incorporation of surface N species, probably in the form of V−N−Al bridges as found accordingly in binary VAlON catalysts.[9] Moreover, different reactions involving N sites of the oxynitride may compete during ammoxidation: (1) N sites move from the bulk to the surface and are partially released as N_2 or transformed to surface NH_x (x = 1−4) sites and (2) N sites are incorporated into the catalyst surface from gaseous NH_3 in the feed. Moreover, a certain loss of the S_{BET} surface area is observed for both samples after use (see Table 1).

At this point it is useful to consider the binding energies of the different surface species in more detail (Table 2, corresponding XP spectra shown in Figure S1 and S2 of Supporting Information [SI]). The E_B values of the Al sites in the fresh catalysts are significantly lower than those reported for Al_2O_3.[17] In VZrAlON-0.5, this might be due to the presence of nitride-like sites in the vicinity of Al (see Discussion below), since the value of 73.8 eV is close to the one observed in AlN (E_B = 73.5−73.6).[18,19] This is also probable for the used VZrAlON-0.1 catalysts, since its surface is significantly populated by N (Table 1). However, for the low Al 2p value in the fresh VZrAlON-0.1 another reason must be responsible since its surface is completely free of N sites. The Zr $3d_{3/2}$ value of 181.1 eV in this catalyst is markedly lower than the one found in ZrO_2 (182.4 eV[20]). This suggests a partial reduction of surface Zr^{4+} to lower-valent Zr species, e.g. Zr^{3+}.[21] A Zr^{3+} species is supposed to attract the electrons in a Zr−O−Al junction weaker than a Zr^{4+} species, which might lead in turn to the lower binding energy for the Al site in this sample. The Zr $3d_{3/2}$ binding energy for the used VZrAlON-0.1 catalyst (181.8 eV) is close to that of the fresh VZrAlON-0.5 sample (182.0 eV). It is higher than expected for Zr^{3+} but lower than for ZrO_2. Considering that the surface of the VZrAlON-0.5 catalyst contains nitrogen, it may be explained by the partial formation of Zr^{4+}−N moieties.

Three different N surface sites with binding energies at 397.6 eV (N1), 401.0 eV (N2), and 403.4 eV (N3) are detected for the fresh VZrAlON-0.5 sample. In agreement with N 1s binding energies of ZrN (397.3−397.6 eV),[22,23] AlN (396.5 eV)[18,19] and VN (397.4 eV),[24] site N1 is assigned to a nitride-like species N^{3-}. Species N2 with E_B values of 400 to 401 eV represent most likely NH_x (x = 1 or 2) sites[25−27] while species N3 might be assigned to NH_4^+.[28] In addition, the presence of NH_4^+ species has been confirmed by FTIR-ATR measurements showing a characteristic vibration at 1400 cm^{-1} (Figure S4 in SI). After ammoxidation the nitride-like species (N1) are no longer seen, and the surface of both used catalysts contains merely NH_x species reflected by E_B values 399.2 and 400.8. Simultaneously, the bulk N content decreases for both samples after use (Table 1). This suggests that N^{3-} species from the bulk move to the surface under reaction conditions where a part of them is transformed into surface NH_x sites while another part might be converted to molecular N_2 as observed accordingly also for several other metal oxynitrides.[29,30] While only one N site is seen in the used sample VZrAlON-0.1, two N sites are detected in the used sample VZrAlON-0.5. This might be due to their coordination to different V sites.

From Table 2 it is evident that the fresh VZrAlON-0.1 catalyst contains only one surface V site, while two of such species are exposed in the fresh sample VZrAlON-0.5. It has been shown previously for a variety of different vanadium oxide samples that reliable information on the mean V valence state can be obtained from the difference of the binding energies of the O 1s and the V $2p_{3/2}$ electrons, $\Delta E_B = E_B(O\ 1s) - E_B(V\ 2p_{3/2})$, rather than from $E_B(V\ 2p_{3/2})$ alone.[31] Those ΔE_B values are shown in Table 2 together with the mean V valence state derived from the correlation between ΔE_B and V valence found for V_xO_y samples in ref 31 (Figure S3 in SI).

It can be seen that the V surface species in the fresh sample VZrAlON-0.1 has a mean valence of 4.3 and is slightly oxidized during ammoxidation to $V^{4.5}$. On the fresh catalyst VZrAlON-0.5 a more reduced site V1 ($V^{3.8}$) and an almost completely oxidized site V2 ($V^{4.8}$) coexist on the surface which get even more reduced and oxidized, respectively, during ammoxidation. This could be an indication that V^{4+} on the surface of this catalyst is depleted under reaction conditions and is transformed into V^{3+} and V^{5+}. A further indication for this may also be derived from in situ EPR measurements discussed below. Based on this result, it is probable that the N species with the lower E_B value (399.2 eV) are connected with V^{3+} sites, while the ones with E_B = 400.8 eV are rather attached to V^{5+}. On the other hand, the single N species in catalyst VZrAlON-0.1 has an intermediate binding energy of 399.5 eV suggesting its location in the vicinity of V^{4+}, which would agree with the presence of the single V surface species detected in this catalyst (Table 2).

dx.doi.org/10.1021/cs500458w | ACS Catal. 2014, 4, 2687−2695

In addition to XPS, EPR and UV−vis diffuse reflectance spectra were recorded to obtain further information on structure and valence states of bulk V sites in fresh VZrAlON catalysts (Figure 3). In the EPR spectra, a multiline signal

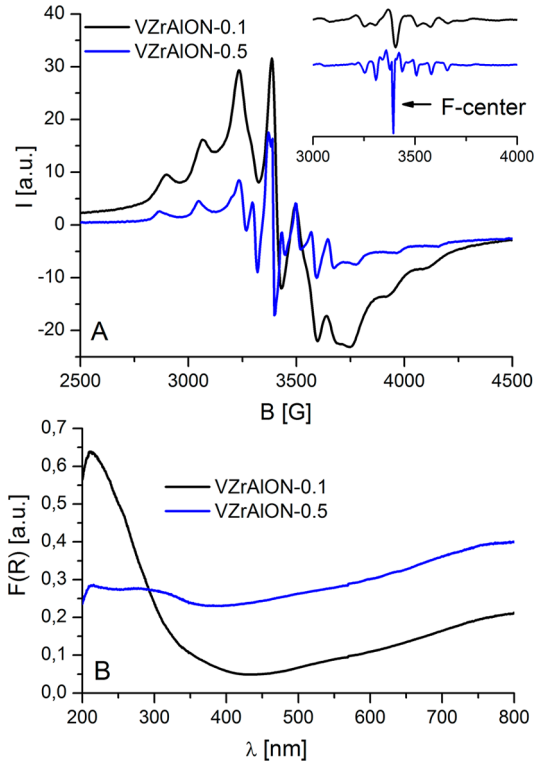

Figure 3. EPR (A) and UV−vis−DR spectra (B) of the fresh catalysts VZrAlON-0.1 and VZrAlON-0.5.

resulting from the hyperfine structure (hfs) coupling of the unpaired electron with the nuclear spin of a V^{4+} single site is superimposed on a broad isotropic background signal which arises from magnetically interacting V^{4+} species. The general shape of the EPR spectra is similar to those of the binary VAlON catalysts in which the V sites were found to be highly dispersed, but it differs significantly from the spectra of the binary VZrON catalysts in which hfs was hardly seen due to dominating polymerized V species.[9] This shows clearly that incorporation of Al into the VZrON network increases the percentage of highly dispersed single V sites. Another interesting feature, which occurs only in the VZrAlON-0.5 but not in the VZrAlON-0.1 catalyst with the lower N content, is a very narrow isotropic line at $g = 2.00$, seen particularly well in the second derivative of the EPR spectrum (Figure 3a, inset). This signal is characteristic for an anionic vacancy occupied by a single electron (also known as F-center).[32,33] Probably, such F-centers are formed during nitridation since this reaction can be formally understood as the replacement of three O^{2-} anions by two N^{3-} anions leaving behind an anionic vacancy which can then accommodate a single electron, possibly from a nearby V^{4+} species as proposed below (eq 5). In catalyst VZrAlON-0.1 with the lower N content, the amount of such defects is obviously not yet high enough to create an EPR signal of sufficient intensity.

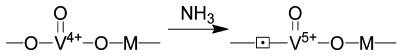

(5)

Among the different possible valence states of vanadium, only V^{4+} is detected by EPR under the given conditions. Despite the higher V content, the total signal intensity of the fresh VZrAlON-0.5 catalyst is much lower compared to VZrAlON-0.1. This can either be due to a higher percentage of V^{5+} or of V^{3+} in the former sample, both species being EPR-silent.

To clarify this issue, UV−vis spectra were recorded (Figure 3B). It has been shown previously that V^{5+} species in oxide catalysts give rise to strong charge-transfer bands in the low wavelength range whereby the band position depends on the coordination number as well as on the agglomeration degree of the V site: CT bands of tetrahedral $V^{5+}O_4$ species appear at lower wavelength than those of octahedral $V^{5+}O_6$ species and a red shift is observed with increasing number of V−O−V bridges.[34] Thus, CT bands of single and polymerized $V^{5+}O_4$ species have been observed below 300 and between 300 and 350 nm, respectively, while those of single and weakly polymerized octahedral $V^{5+}O_6$ species fall around 400 nm respectively between 400 and 430 nm.[35,36] For V_2O_5 nanocrystallites with the highest polymerization degree, light absorption extends into the visible range up to 485 nm, due to delocalized acceptor levels.[37] Bands arising from d-d transitions of reduced V^{4+} and V^{3+} species are usually broad and less intense compared to CT bands of V^{5+} since such d-d transitions are frequently symmetry-forbidden. Thus, d-d transitions of the $VO(H_2O)_5^{2+}$ complex ion fall at 365, 609, and 840 nm[38] while they have been observed at 625 and 769 nm in V-silicalite.[34a] d-d transitions of V^{3+} in vanadium phosphates occurred at 980, 694, and 444 nm in the case of $V(PO_3)_3$[39] as well as at 500 nm in case of reduced $(VO)_2P_2O_7$.[40] From this consideration it is readily evident that in V-containing solid catalysts a distinct assignment of absorbance in the high wavelength range to specific d-d transitions of V^{4+} and V^{3+} is very difficult when both species superimpose in the UV−vis spectrum. This is the reason why frequently only a more or less featureless increase of absorbance is observed above 400 nm in partially reduced V-containing solids.[41] This is also evident from the UV−vis spectra of VZrAlON catalysts in Figure 3B. The spectrum of VZrAlON-0.1 is dominated by a strong charge-transfer band of V^{5+} below 300 nm, pointing to the dispersed character of the V sites, and a slight increase of absorbance above 400 nm which confirms the presence of some reduced V species. In sample VZrAlON-0.5 with the higher V content, yet the smaller EPR signal (Figure 3A) light absorption is most pronounced in the higher wavelength range above 400 nm which indicates the presence of reduced V^{4+} and V^{3+} species. Although, as explained above, a clear distinction of these both valence states just based on UV−vis spectra is not possible, comparison of UV−vis and EPR spectra suggests that the lower total EPR intensity of sample VZrAlON-0.5 might not be related to V^{5+} (which should contribute to the CT band intensity below 400 nm) but to V^{3+}, which contributes to the absorbance above 500 nm in the UV−vis spectrum of Figure 3B but not to the corresponding EPR spectrum in Figure 3A. This is confirmed, too, by XPS for the catalyst surface (Table 2).

The spin Hamiltonian parameters $g_\parallel$ $g_\perp$, $A_\parallel$ and $A_\perp$ derived by spectra simulation for the single VO^{2+} sites (Table 3) can provide information on differences of their local environment in the two catalysts. The quotient $\Delta g_\parallel/\Delta g_\perp$ (eq 3) is a measure for the axial distortion of the VO^{2+} site; the higher this value, the shorter the axial V=O bond and/or the longer the equatorial V−O bonds of the VO^{2+} site. The in-plane

dx.doi.org/10.1021/cs500458w | ACS Catal. 2014, 4, 2687−2695

Table 3. Spin Hamilton parameters $g_{\|}$, $g_{\perp}$, $A_{\|}$, $A_{\perp}$, $\Delta g_{\|}/\Delta g_{\perp}$ (eq 3) and In-Plane Delocalization Coefficients $\beta_2{}^{*2}$ (eq 4) for Single VO^{2+} Derived from EPR Spectra Simulation (for a comparison of selected experimental and simulated spectra see SI, Figure S5); Parameters for the Broad Isotropic Background and the F Center Signal Are Not Included

sample	$A_{\|}$ [G]	$A_{\perp}$ [G]	$g_{\|}$	$g_{\perp}$	$\Delta g_{\|}/\Delta g_{\perp}$	$\beta_2{}^{*2}$
			VZrAlON-0.1			
fresh, 20 °C	−176	−54	1.936	1.962	1.65	0.71
air/NH_3, 350 °C	−176	−55	1.935	1.968	1.94	0.70
air/NH_3/H_2O/3-PIC, 350 °C	−187	−66	1.923	1.978	3.20	0.69
air/NH_3, 350 °C	−177	−55	1.935	1.968	1.94	0.70
N_2, 350 °C	−177	−58	1.933	1.970	2.14	0.68
N_2, 20 °C	−177	−53	1.939	1.962	1.58	0.72
			VZrAlON-0.5			
fresh, 20 °C						
site 1	−193	−61	1.920	1.968	2.41	0.75
site 2	−180	−72	1.930	1.966	2.01	0.61
air/NH_3, 350 °C	−181 (−183)[a]	−64 (−65)[a]	1.921 (1.932)[a]	1.976 (1.981)[a]	3.10 (3.30)[a]	0.66 (0.67)[a]
air/NH_3/H_2O/3-PIC, 350 °C	−183	−64	1.920	1.976	3.10	0.67
air/NH_3, 350 °C	−184	−64	1.920	1.973	3.10	0.67
N_2, 350 °C	−176	−63	1.914	1.972	3.28	0.65
N_2, 20 °C	−182	−61	1.921	1.973	2.73	0.69

[a]Values in brackets taken from ref 9 for the binary VAlON-0.5 catalyst under the same conditions.

delocalization coefficient $\beta_2{}^{*2}$ (eq 4) reflects the extent to which the single electron is delocalized away from the V center toward the ligands in the basal plane of the VO^{2+} site. For a pure VO^{2+} ion, $\beta_2{}^{*2}$ is equal to unity and decreases with electron delocalization, i. e., with rising covalent character of the V-ligand bonds in the basal plane.

While the experimental EPR spectrum of the fresh VZrAlON-0.1 catalyst reflects only one type of single VO^{2+} site, two of such species S1 and S2 are present in sample VZrAlON-0.5 (Table 3). The ratio of their relative intensities S2/S1 = 1.6 is almost equal to the Al/Zr ratio. This could suggest that site 1 may be connected with Zr, while site 2 may be rather localized in the vicinity of Al. This is also supported by the similarity of the spin Hamiltonian parameters of site 2 with those observed for single VO^{2+} species in the binary VAlON-0.5 given in brackets in Table 3. Apart from the X-ray-amorphous nature of the catalysts, this is another hint for the presence of a well intermixed V−Al−N(O)−Zr network.

In Situ EPR Studies during Nitridation. To follow the evolution of the V sites during nitridation, the oxide precursor VZrAlO-0.5 was first heated in N_2 flow from 20 to 120 °C before switching to 20% NH_3/N_2. EPR spectra have been recorded until reaching a steady state before the temperature was ramped to the next level. From Figure 4 it can be seen that the total EPR signal intensity increases strongly upon raising the temperature from 120 to 300 °C and decreases again upon further heating to 410 °C. This points to a gradual reduction of EPR-silent V^{5+} in the fresh oxide precursor, first to EPR-active V^{4+} at moderate temperature and further to EPR-silent V^{3+} at 410 °C. At this temperature, also the narrow F-center signal appears, confirming that the formation of these vacancies is indeed a consequence of increasing replacement of O by N.

Most likely, the F-centers are located in the vicinity of V^{5+} centers, since the magnetic interaction with the unpaired d-electrons of V^{4+} and/or V^{3+} sites would broaden the line beyond detection. Considering the fact that these F-centers are only formed with increasing incorporation of N species and the latter are themselves stabilized by V, it may be assumed that a process depicted in eq 5 occurs during nitridation, in which ⊡ denotes an oxygen vacancy occupied by a single electron (F-center) and M is Al or Zr.

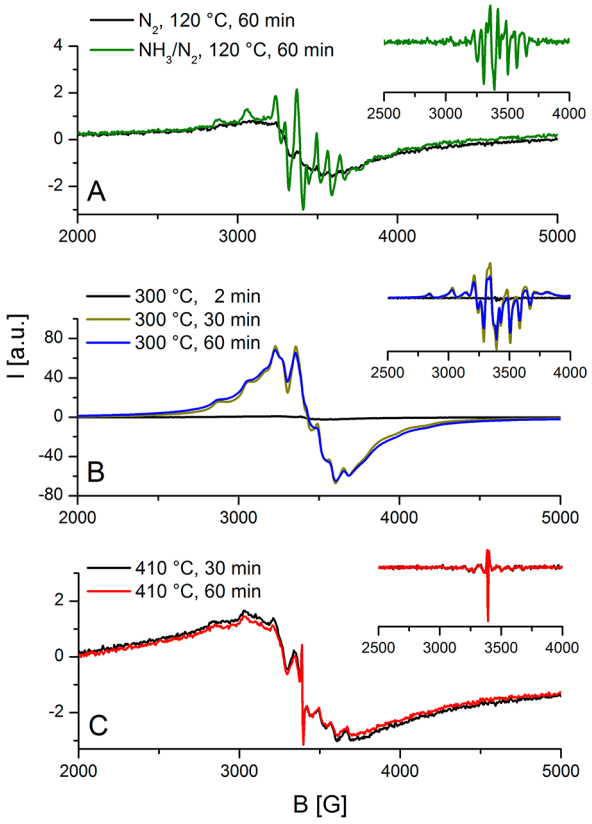

Figure 4. EPR spectra measured during nitridation of the VZrAlO-0.5 oxide precursor: (A) at 120 °C after heating the sample in N_2 followed by 1 h treatment in 20% NH_3/N_2 flow, (B) as a function of time after reaching T = 300 °C in 20% NH_3/N_2 flow, and (C) as a function of time after reaching T = 410 °C in 20% NH_3/N_2 flow.

In Situ EPR Studies during Ammoxidation. To probe the impact and role of paramagnetic sites in the oxynitrides during the catalytic reaction, in situ EPR measurements of samples VZrAlON-0.1 and VZrAlON-0.5 have been performed

dx.doi.org/10.1021/cs500458w | ACS Catal. 2014, 4, 2687−2695

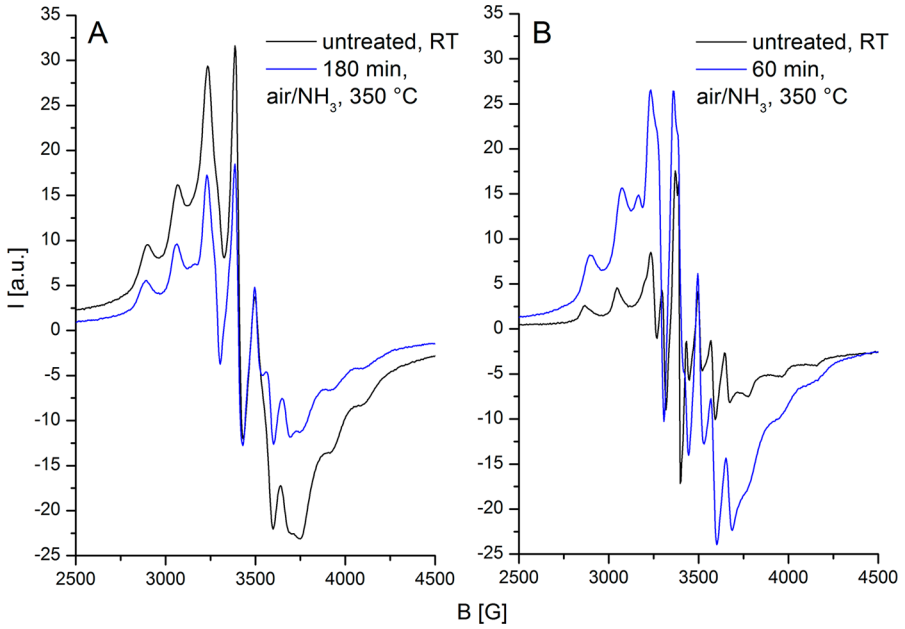

Figure 5. EPR spectra of the as-prepared catalysts VZrAlON-0.1 (A) and VZrAlON-0.5 (B) Recorded at RT and after heating in air/NH_3 (5.6/1) flow to the reaction temperature of 350 °C.

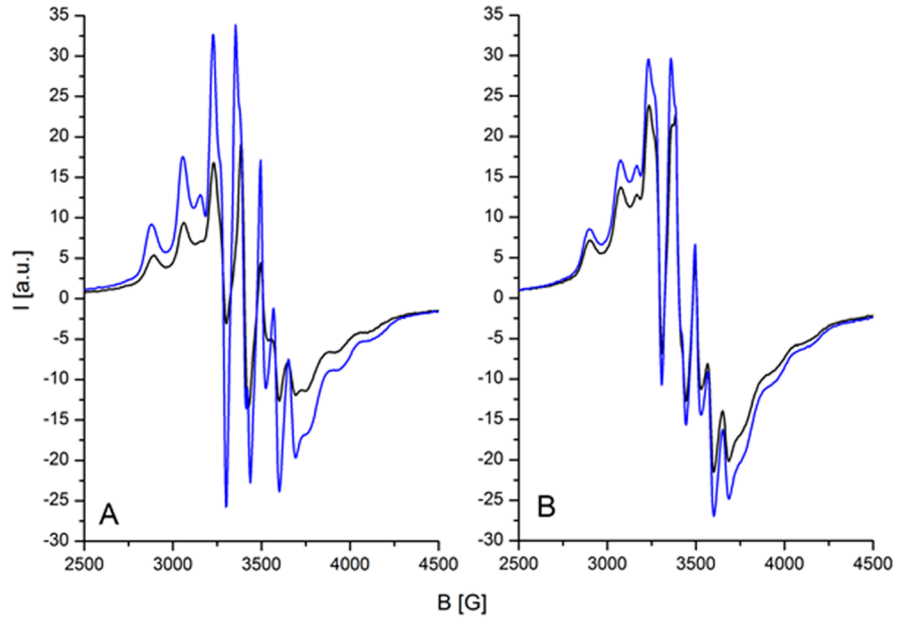

Figure 6. EPR spectra of VZrAlON-0.1 (A) and VZrAlON-0.5 (B) recorded at 350 °C under air/NH_3 (black, identical with blue spectra in Figure 5) and after subsequent treatment for 45 min in the total feed (3-PIC/air/NH_3/H_2O = 1/30/6/8) at 350 °C.

during subsequent treatment with feed components. The catalysts have been first heated in air/NH_3 (4.5/1) flow to the reaction temperature of 350 °C (Figure 5). Then subsequently H_2O and 3-PIC have been added to the feed stream at 350 °C (3-PIC/air/NH_3/H_2O = 1/28/5/8) (Figure 6). After reaching a steady state, H_2O and 3-PIC were removed from the feed again.

A significant difference between the two catalysts is already evident upon heating in air/NH_3 flow to the reaction temperature of 350 °C (Figure 5), since the total EPR signal intensity decreases for VZrAlON-0.1, while it increases for VZrAlON-0.5. In the former case, the loss of intensity might be just a temperature effect, since Curie's law predicts an intensity ratio I(350 °C)/I(20 °C) of 0.5, which is indeed the case for VZrAlON-0.1, suggesting that the concentration of V^{4+} in the sample remains constant during heating in air/NH_3. In contrast, the EPR intensity of sample VZrAlON-0.5 increases strongly (Figure 4b). This indicates that V^{3+} sites formed upon nitridation are at least partially reoxidized in air/NH_3 flow at 350 °C. Moreover, the spin Hamiltonian parameters in Table 3 indicate that the local structure of the VO^{2+} sites in VZrAlON-0.1 remains almost unchanged during this treatment, while significant changes of VO^{2+} sites are detected in VZrAlON-0.5. This catalyst contains two different VO^{2+} single sites in its initial state, but site 1 (tentatively assigned as attached to Zr) is no longer seen after treatment in air/NH_3, probably due to

dx.doi.org/10.1021/cs500458w | ACS Catal. 2014, 4, 2687−2695

oxidation. In accordance with the strong intensity increase (Figure 4b) and the similarity of spin Hamiltonian parameters of site 2 with those of the binary VAlON-0.5 catalyst (values in brackets in Table 3), in can be concluded that V^{3+} sites in the vicinity of Al are reoxidized and stabilized as VO^{2+} while those in the vicinity of Zr might be converted to VO^{3+}. This agrees well with previous observations on binary VZrON catalysts, in which V sites were found to prefer a valence state of +5 under reaction conditions.[9] From Table 3 it is evident that the quotient $\Delta g_{\parallel}/\Delta g_{\perp}$ of sites 2 increases during treatment in air/NH_3, indicating that their local geometry becomes more distorted. This could suggest that already under these conditions nitride-like sites are transformed to NH_x sites as also indicated by XPS results. In addition, also the concentration of F-centers decreases. This is evident from the ratio of the intensities of the subsignals needed to reproduce the experimental EPR spectrum of catalyst VZrAlON-0.5 in air/NH_3 flow at 350 °C. The relative contribution of the F-center signal to the total EPR intensity decreases by a factor of about 6. A possible reason may be that gas-phase oxygen takes up the electrons in these vacancies upon adsorption and is converted into O^{2-} ions (eq 6) which fill the vacancies.[42] The reverse process would restore the F-centers and liberate oxygen which then reacts with 3-PIC. This is the well-known Mars–van Krevelen mechanism.

$$O_2 \overset{e^-}{\leftrightarrows} O_2^- \overset{e^-}{\leftrightarrows} O_2^{2-} \leftrightarrows 2O^- \overset{2e^-}{\leftrightarrows} 2O^{2-} \quad (6)$$

A similar behavior was observed for F-centers in an amorphous iron vanadate phase which catalyzed the selective gas-phase oxidation of fluorene to 9-fluorenone very selectively. The high selectivity was attributed to the fast conversion of nonselective electrophilic oxygen intermediates to nucleophilic oxide ions able to insert into the aromatic ring without destroying it.[43]

When H_2O is added to the air/NH_3 flow at 350 °C, the EPR spectra did not change and are therefore not shown. However, upon admixing 3-PIC, which results in the complete feed mixture (3-PIC/air/NH_3/H_2O = 1/30/6/8), the EPR signal rises strongly for sample VZrAlON-0.1 but only marginally for sample VZrAlON-0.5 (Figure 6). This intensity increase is most probably due to the reduction of V^{5+} to V^{4+} by 3-PIC which itself is oxidized in turn. The spin Hamiltonian parameters of the VO^{2+} site in sample VZrAlON-0.1 point to an increasing distortion of the local environment, reflected by a rise of the $\Delta g_{\parallel}/\Delta g_{\perp}$ ratio from 1.94 to 3.20, which is completely reversible when H_2O and 3-PIC are removed from the feed again (Table 3). Given the fact that H_2O caused no changes of the VO^{2+} sites, this suggests that the (amm)oxidation product of 3-PIC is adsorbed on the latter.

In contrast to VZrAlON-0.1, the total EPR intensity increases only very slightly and the spin Hamiltonian parameters of the VO^{2+} sites do not change at all (Table 3). This indicates that the local environment of these sites remains unchanged upon contact of the catalyst surface with 3-PIC, probably, since they are not exposed on the surface. This would agree with the XPS results, which show that the two kinds of surface V species are mainly trivalent and pentavalent, respectively, but not tetravalent (Table 2).

Mechanistic Considerations. Previously it was found that ammoxidation of methylaromatics proceeds very effectively on vanadyl pyrophosphate that contains O-bridged ladder-like double chains of VO^{2+} sites.[37] The proposed reaction mechanism implies the adsorption of the aromatic ring at a Lewis surface site followed by H abstraction from the CH_3 group at the neighboring $V^{n+}{=}O$ surface site, which gets reduced to $V^{(n-1)+}{-}OH$. It is clear that such a step is not probable on a V^{3+} surface site since reduction to V^{2+} might be energetically unfavorable. Therefore, V^{3+} surface species can be ruled out as active sites, as it was also shown experimentally.[44] The conversion of $-CH_3$ to $-CHO$ and further to $-C{\equiv}N$ implies the participation of lattice O and N and, consequently, requires several subsequent reduction/reoxidation cycles of the involved vanadyl site (see Figure 9 in ref 37). It has been concluded that the periodic electronic distortion of this vanadyl site is diminished by delocalization of its electron density within the respective vanadyl chain, which was considered as a major reason for the beneficial catalytic effect of interconnected VO^{2+} structural units.

Given that the same reaction mechanism holds also for the ammoxidation of 3-PIC on VZrAlON-0.5, the active sites should provide functions similar to those in vanadyl pyrophosphate, namely a Lewis site for adsorption of the aromatic ring with a nearby redox-active vanadyl site that can delocalize its fluctuating electron density. This may be realized in a proper way by the $-\boxdot-V^{5+}(O)-N-Al(Zr)-$ moiety formed upon nitridation in VZrAlON-0.5, but not in the poorly active VZrAlON-0.1catalyst (eq 5). In the mechanism proposed in ref 37 it is assumed that the methyl group of the substrate is first oxidized to adsorbed aldehyde which subsequently reacts with surface NH_4^+ species. It is probable that N within the surface $-\boxdot-V^{5+}(O)-N-Al(Zr)-$ moiety represents an NH_x species, which may react with an aldehyde intermediate according to the mechanism in ref 37. The XPS results point to a dynamic behavior of the N species during reaction which may be promoted by H_2O in the feed. It was found that, on the one hand, N sites move from the bulk to the surface where they are partially converted to surface NH_x (x = 1–4) sites, and on the other hand, such sites are formed by interaction of the surface with gaseous NH_3 in the feed.

The F-center ($\boxdot$) can activate gas-phase oxygen (eq 6), Al and/or Zr can act as Lewis adsorption sites, while the $V^{5+}{=}O$ can abstract H from CH_3 in the initial step, forming $V^{4+}{-}OH$. V^{4+} can delocalize its electron to the neighboring vacancy (restoring the F-center for another redox cycle) after O and N leave their surface sites for reaction with the adsorbed intermediate.

CONCLUSIONS

We have developed a new class of ternary VZrAlON oxynitrides for the ammoxidation of 3-picoline to 3-cyanopyridine which combine the beneficial properties of the highly active but poorly selective VZrON and the highly selective but poorly active VAlON binary counterparts, namely an activity which is only slightly lower than that of VZrON and a selectivity almost as high as that obtained with VAlON. With the best VZrAlON-0.5 catalyst, the highest space-time yield ever measured in gas-phase ammoxidation of 3-PIC to 3-CP (STY = 488 g L^{-1} h^{-1}) has been obtained, which is markedly higher than our best previous result for VZrON-0.25 (STY = 399 g L^{-1} h^{-1})[9] and all the more that of the industrial SbVTiSiXO benchmark catalyst (STY = 150 g L^{-1} h^{-1}).[10] This might be due to the following reasons:

In comparison to VZrON materials, which contain no surface nitrogen and are dominated by crystalline ZrO_2 and $V_x^{5+}O_y$ clusters,[9] the addition of Al to the ZrO matrix prevents crystallization of ZrO_2 and leads to an X-ray-amorphous well-

mixed Al−O−Zr network which incorporates preferentially highly dispersed vanadyl sites and exposes surface N sites. In addition to a mean surface V valence close to +4, the latter two features were previously related to the high selectivity of VAlON catalysts[9] and might be responsible, too, for the improved selectivity of the present VZrAlON-0.5 catalyst. In contrast to the less active VAlON-0.5 catalyst, which contained V^{4+} and V^{3+} but no V^{5+} surface sites,[9] the surface of VZrAlON-0.5 exposes mainly V^{5+} and V^{3+} but no V^{4+}. V^{3+} surface sites are inactive in both cases. Thus, one reason for the improved activity of the VZrAlON-0.5 catalyst might be, apart from the somewhat higher surface area (S_{BET} =153 m^2 g^{-1} for VZrALON vs 98 m^2 g^{-1} for VAlON), the exposure of V^{5+} which has a higher redox potential than V^{4+}. However, in contrast to VZrON, which exposes abundant V^{5+} besides some V^{4+} (mean V valence = 4.7) mainly in the form of V_xO_y clusters,[9] the active V^{5+} surface sites on VZrALON-0.5 are separated by inactive V^{3+} species (mean V valence = 4.2) as evidenced by XPS. This "dilution" might be a reason why total oxidation is suppressed. It is anticipated that the junction of a V^{5+} site with an F-center and a nearby N species on the surface of VZrAlON-0.5 provides optimum conditions for double Mars−van Krevelen mechanism which requires both the activation of gas-phase oxygen and ammonia via reversible incorporation into the catalyst surface as well as an efficient electron transport, the latter being realized by shuttling electrons between V^{5+}, the F-centers, and the reactants.

■ ASSOCIATED CONTENT

Supporting Information

XPS spectra and data, ATR-FTIR spectra, calculated EPR spectra. This material is available free of charge via the Internet at http://pubs.acs.org.

■ AUTHOR INFORMATION

Corresponding Author

*E-mail: angelika.brueckner@catalysis.de

Notes

The authors declare no competing financial interest.

■ ACKNOWLEDGMENTS

The authors thank Deutsche Forschungsgemeinschaft (Grant No. BR 1380-15-1) and Max-Buchner-Forschungsstiftung for financial support.

■ REFERENCES

(1) Grasselli, R. K.; Trifirò, F.; Forni, L. In *Handbook of Heterogeneous Catalysis*, 2nd ed.; Ertl, G., Knözinger, H., Schüth, F., Weitkamp, J., Eds.; Wiley-VCH, Weinheim, 2008; Vol. 7, p 3517.

(2) Lücke, B.; Martin, A. In *Fine Chemicals through Heterogeneous Catalysis*, 1st ed.; Sheldon, R., van Bekkum, H., Eds.; Wiley-VCH, Weinheim, 2001, 527.

(3) Centi, G.; Perathoner, S. *Catal. Rev. Sci. Eng.* **1998**, *40*, 175−208.

(4) Martin, A.; Hannour, F. K.; Brückner, A.; Lücke, B. *React. Kinet. Catal. Lett.* **1998**, *63*, 245−251.

(5) Martin, A.; Lücke, B. *Catal. Today* **2000**, *57*, 61−70.

(6) Narayana, K. V.; Venugopal, A.; Rama Rao, K. S.; Venkat Rao, V.; Masthan, S. K.; Kanta Rao, P. *Appl. Catal., A* **1997**, *150*, 269−278.

(7) Sai Prasad, P. S.; Lingaiah, N.; Khaja Masthan, S.; Rama Rao, K. S.; Kanta Rao, P. *Catal. Lett.* **1996**, *36*, 195−199.

(8) Martin, A.; Narayana Kalevaru, V.; Lücke, B.; Brückner, A. *Appl. Catal., A* **2008**, *335*, 196−203.

(9) Janke, C.; Radnik, J.; Bentrup, U.; Martin, A.; Brückner, A. *ChemCatChem.* **2009**, *1*, 485−491.

(10) Hippel, L. v.; Neher, A.; Amtz, D. (Degussa-Hüls AG). EP 0726092 B1 1999.

(11) Martin, A.; Zhang, Y.; Zanthoff, H. W.; Meisel, M.; Baerns, M. *Appl. Catal., A* **1996**, *139*, L11−16.

(12) Janke, C.; Schneider, M.; Bentrup, U.; Radnik, J.; Martin, A.; Scholz, G.; Brückner, A. *J. Catal.* **2011**, *277*, 196−207.

(13) Brückner, A. *Chem. Commun.* **2005**, *13*, 1761−1763.

(14) Lozos, G. P.; Hofman, B. M.; Franz, C. G. Quantum Chemistry Program Exchange; 1973; 265.

(15) Novinska, K.; Wieckowski, A. *Z. Phys. Chem, Neue Folge* **1989**, *162*, 231−244.

(16) McGarvey, B. R. *J. Phys. Chem.* **1967**, *71*, 51−67.

(17) Hess, A.; Kemnitz, E.; Lippitz, A.; Unger, W. E. S.; Menz, D. H. *J. Catal.* **1994**, *148*, 270−280.

(18) Liu, H.; Bertolet, D. C.; Rogers, J. W., Jr. *Surf. Sci.* **1995**, *340*, 88−100.

(19) Rosenberger, L.; Baird, R.; McCullen, E.; Auner, G.; Shreve, G. *Surf. Interface Anal.* **2008**, *40*, 1254−1261.

(20) Chris, B. V. In *Handbooks of Monochromatic XPS Spectra*; XPS International LLC: Mountain View, 2005; Vol. 2, p 828.

(21) Wang, Q. M.; Gong, J.; Sun, C.; Lee, H. W.; Kim, K. H. *J. Ceram. Proc. Res.* **2011**, *12*, 259−264.

(22) Prieto, P.; Galán, L.; Sanz, J. M. *Surf. Interface Anal.* **1994**, *21*, 395−399.

(23) Milošev, I.; Strehblow, H. H.; Gaberščcek, M.; Navinšek, B. *Surf. Interface Anal.* **1996**, *24*, 448−458.

(24) Hendrickson, D. N.; Hollander, J. M.; Jolly, W. L. *Inorg. Chem.* **1969**, *8*, 2642−2647.

(25) Wiame, H.; Bois, L.; Lharidon, P.; Laurent, Y.; Grange, P. *Solid State Ionics* **1997**, *101−103*, 755−759.

(26) Truica-Marasescu, F.; Wertheimer, M. R. *Plasma Proc. Polym.* **2008**, *5*, 44−57.

(27) Ando, R. A.; do Nascimento, G. M.; Landers, R.; Santos, P. S. *Spectrochim. Acta, Part A* **2008**, *69*, 319−326.

(28) Florea, M.; Prada Silvy, R.; Grange, P. *Appl. Catal., A* **2005**, *286*, 1−10.

(29) Wiame, H.; Centeno, M.-A.; Picard, S.; Bastians, P.; Grange, P. *J. Eur. Ceram. Soc.* **1998**, *18*, 1293−1299.

(30) Le Gendre, L.; Marchand, R.; Laurent, Y. *J. Eur. Ceram. Soc.* **1997**, *17*, 1813−1818.

(31) Mendialdua, J.; Casanova, R.; Barbaux, Y. *J. Electron Spectrosc. Relat. Phenom.* **1995**, *71*, 249−261.

(32) Cooke, D. W.; Blair, M. W.; Smith, J. F.; Bennett, B. L.; Jacobsohn, L. G.; McKigney, E. A.; Muenchausen, R. E. *IEEE Trans. Nucl. Sci.* **2008**, *55*, 1118−1122.

(33) Schimpf, S.; Lucas, M.; Mohr, C.; Rodemerck, U.; Brückner, A.; Radnik, J.; Hofmeister, H.; Claus, P. *Catal. Today* **2002**, *72*, 63−78.

(34) Burcham, L. J.; Deo, G.; Gao, X.; Wachs, I. E. *Top. Catal.* **2000**, *11−12*, 85−100.

(35) Centi, G.; Perathoner, S.; Trifiro, F.; Aboukais, A.; Aissi, C. F.; Guelton, M. *J. Phys. Chem.* **1992**, *96*, 2617−2629.

(36) Brückner, A.; Rybarczyk, P.; Kosslick, H.; Wolf, G.-U.; Baerns, M. *Stud. Surf. Sci. Catal.* **2002**, *142*, 1141−1148.

(37) Morey, M.; Davidson, A.; Eckert, H.; Stucky, G. *Chem. Mater.* **1996**, *8*, 486−492.

(38) Ballhausen, C. J.; Gray, H. B. *Inorg. Chem.* **1962**, *1*, 111−122.

(39) Rojo, J. M.; Mesa, J. L.; Lezama, L.; Rojo, T.; Olazcuaga, R.; Guillen, F. *Ann. Chim. Sci. Mater.* **1998**, *23*, 107−l 11.

(40) Cavani, F.; Ligi, S.; Monty, T.; Pierelli, F.; Trifirò, F.; Albonetti, S.; Mazzoni, G. *Catal. Today* **2000**, *61*, 203−210.

(41) Brückner, A.; Kondratenko, E. *Catal. Today* **2006**, *113*, 16−24.

(42) Bielanski, A.; Haber, J. *Oxygen in Catalysis*; Marcel Dekker: New York, 1991; p 150.

(43) Bruckner, A.; Wolf, G. U.; Meisel, M.; Stosser, R.; Mehner, H.; Majunke, F.; Baerns, M. *J. Catal.* **1995**, *154*, 11−23.

(44) Brückner, A. *Catal. Rev. Sci. Eng.* **2003**, *45*, 97−150.